IEEE Photonics Journal
An IEEE Photonics Society Publication

Open Access

Behavioral Modeling of Photon Arrival Time for Time-of-Flight Measurement Circuit Simulation

Volume 11, Number 1, February 2019

Yue Xu, *Member, IEEE*
Zhong Wu
Ding Li

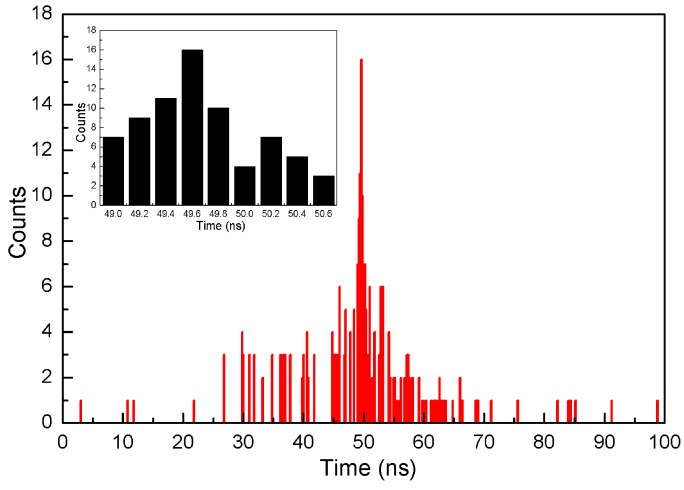

DOI: 10.1109/JPHOT.2019.2893351
1943-0655

Behavioral Modeling of Photon Arrival Time for Time-of-Flight Measurement Circuit Simulation

Yue Xu,[1,2] ***Member, IEEE***, **Zhong Wu**,[1] **and Ding Li**[1]

[1]College of Electronic and Optical Engineering and the College of Microelectronics, Nanjing University of Posts and Telecommunications, Nanjing 210023, China
[2]National and Local Joint Engineering Laboratory of RF Integration and Micro-Assembly Technology, Nanjing 210023, China

DOI:10.1109/JPHOT.2019.2893351

Manuscript received November 5, 2018; revised January 3, 2019; accepted January 12, 2019. Date of publication January 16, 2019; date of current version January 31, 2019. This work was supported in part by the National Natural Science Foundation of China (61571235 and 61871231), in part by the Natural Science Foundation of Jiangsu Province, China (BK20181390), and in part by the QingLan Project of Jiangsu Province Colleges, China. Corresponding author: Yue Xu (e-mail: xuyue_cd@163.com).

Abstract: This letter proposes a behavioral model to estimate the statistical photon arrival time for time-of-flight (TOF) measurement circuit simulation. A theoretical model is derived to calculate the photon arrival rate by full consideration of a variety of properties of a TOF measurement system, such as laser source, optics, single-photon avalanche diode detector, target distance, and ambient illumination. For the first time, the newly developed model is implemented in behavioral Verilog-A hardware description language and successfully operated on Cadence Spectre simulator for TOF circuit simulation. It is capable of accurately predicting the statistical performance parameters such as photon arrival time and achievable distance, providing a new candidate tool for the ease of design and simulation of various high-performance TOF measurement circuits.

Index Terms: Behavioral model, time-of-flight (TOF), single-photon avalanche diode (SPAD), ambient illumination.

1. Introduction

In the past decade years, laser imaging detection and ranging (LIDAR) technique has become a promising method to offer precise distance and spatial resolution measurements by means of time-of-flight (TOF) principle [1], [2]. Due to high sensitivity and picosecond timing resolution, single photon avalanche diodes (SPADs) fabricated in low-cost CMOS technology have attracted great interest in the time-correlated LIDAR systems [3], [4]. For instance, one potential application of CMOS SPAD-based imagers is in advanced driver assistance systems (ADAS), which enables the automotive three-dimensional (3D) vision through the TOF technique [5]–[7].

A typical SPAD-based LIDAR system mainly consists of a laser transmitter, a few optical components, a system control circuit and a SPAD imager integrated with a time-to-digital converter (TDC) or a time-to-amplitude converter (TAC) and other on-chip electronics for photon timing [8]–[10]. The TDC or TAC as a key TOF measurement circuit, in order to better understand their performance and further predict the error of TOF measurement information, an accurate behavioral model for simulating the statistical photon arrival time is in great demand.

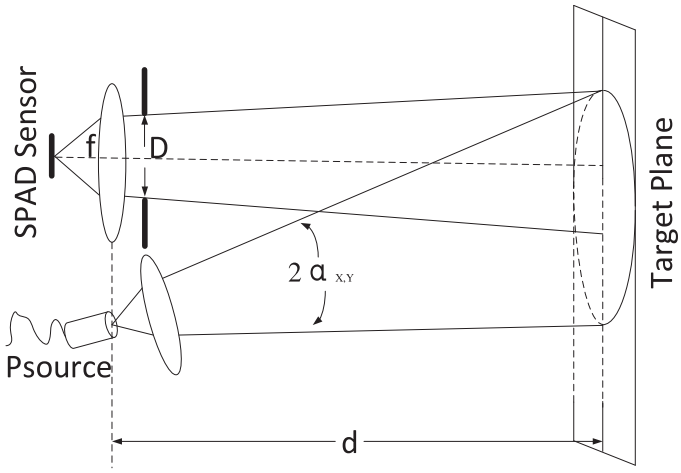

Fig. 1. Schematic of the light path in a LIDAR measurement system.

Some theoretical models have been presented to estimate the rate of photons impinging on SPAD devices [11]–[13]. The key LIDAR system parameters like the laser source, the target object, and the ambient light are taken into account in these models. On the basis of the theoretical models, Monte Carlo simulation is usually carried out to assess the performance of a SPAD-based LIDAR system, such as ranging precision and immunity to ambient light [11], [12], [14]. However, since the theoretical models cannot be directly applied in the LIDAR system level circuit simulation, the timing performance of the TOF measurement circuit cannot be accurately analyzed. Moreover, the presented Monte Carlo simulation doesn't fully consider various non-ideal factors, for example, the jitter time of laser and the timing resolution and nonlinearity of TDC circuits, thus the simulation results are too idealized to evaluate the performance of the whole LIDAR system comprehensively.

The focus of this work is to develop a novel behavioral simulation model, which is used to estimate the statistical photon arrival time for SPAD detectors. For the first time, the behavioral model has been implemented in Verilog-A hardware description language (HDL) and the TOF measurement circuit simulation has been available run on the commercial simulator. Since the TOF circuit simulation involves a variety of influences of photons arrival time, SPAD device, quenching and TDC circuits, the desired distance information can be accurately predicted. The proposed behavioral simulation model provides a promising candidate tool for the developments of the SPAD-based TOF sensors.

2. Modeling of Photon Arrival Time

The rate of a photon incident on the SPAD sensor for a given optical source power is firstly calculated according to the photon flight path. Fig. 1 illustrates a typical photon flight path in a LIDAR measurement system where a light beam emitted by a laser source is reflected by the target and then sensed by the SPAD detector.

For a point-like laser source with optical power P_{Source}, if the light beam is emitted with divergence angles of α_x and α_y in horizontal and vertical directions, respectively, we can calculate the optical power density at the target distance d as [11]

$$E_{Source} = \frac{P_{Source}}{d^2 4 \cdot \arcsin(\sin\alpha_x \cdot \sin\alpha_y)} \tag{1}$$

On the other hand, the area of the view field at the distance d can be expressed with

$$A_{FoV} = 4d^2 \cdot \tan(FoV_x/2) \cdot \tan(FoV_y/2) \tag{2}$$

Here, the horizontal and vertical view angles FoV_x and FoV_y are respectively given by [4]

$$FoV_x = 2\tan^{-1}\left(\frac{L}{2f}\right) \tag{3}$$

$$FoV_y = 2\tan^{-1}\left(\frac{W}{2f}\right) \tag{4}$$

In which, f is the lens focal length, L and W are the length and width of the pixel pitch of the SPAD detector, respectively. The area of a pixel equals to $A_{pix} = L \times W$.

It can be seen that the product term of the $E_{source}A_{FoV}$ represents the incident light power on the view field. The power density of the return laser beam reflected by the target in the field of view is decreased with the square of the distance by the term $1/2\pi d^2$. Further considering the reflectance coefficient Γ_T of the target and the transmission losses T_0 of the laser and optical lens, we can obtain the optical power focused on the SPAD detector as

$$P_{pixel} = E_{Source} \cdot A_{FoV} \cdot \frac{1}{2\pi d^2} \cdot \Gamma_T \cdot T_0 \cdot A_{aperture} \tag{5}$$

Where the $A_{aperture}$ is defined as the area of a lens with an optical aperture D and it is given by

$$A_{aperture} = \pi\frac{D^2}{4} \tag{6}$$

In order to estimate the photo incidence rate on the SPAD detector, the optical power per pixel in Equation (5) should be divided by the single photon average energy hc/λ. Here, h is the Planck's constant, c is the speed of light, and λ is the wavelength. In addition, the fill factor (FF) and the photon detection efficiency (PDE) of the SPAD detector should be also considered. Finally, the laser photon arrival rate can be calculated by

$$R_{Laser} = \frac{E_{Source} \cdot D^2 \cdot \Gamma_T \cdot T_o \cdot A_{pix} \cdot \lambda \cdot FF \cdot PDE}{8 \cdot f^2 \cdot h \cdot c} \tag{7}$$

However, besides laser photons, the ambient photons are also detected by the SPAD sensor at the same time, which inevitably has a serious impact on the detectable precision of LIDAR measurement system. Accordingly, the ambient illumination must be included in the total photon detection rate as well. In fact, an optical bandpass filter is generally used to eliminate the light illumination outside the filter band, thus the ambient light power density is obtained with

$$E_{Amb} = \int_{\lambda-\Delta\lambda}^{\lambda+\Delta\lambda} E_{sun}(\lambda')d\lambda' \tag{8}$$

Where the $E_{sun}(\lambda')$ is the power density spectrum of ambient illumination through the optical bandpass filter. By replacing E_{Source} with E_{Amb} in Equation (7), we can acquire the ambient photon arrival rate as follows:

$$R_{Amb} = \frac{E_{Amb} \cdot D^2 \cdot \Gamma_T \cdot T_o \cdot A_{pix} \cdot \lambda \cdot FF \cdot PDE}{8 \cdot f^2 \cdot h \cdot c} \tag{9}$$

As seen from the Equation (9), the ambient photon detection rate is irrelevant with the target distance but depends on the LIDAR optical system parameters and the SPAD detector characteristics.

It is worth noting that the statistic photon arrival time exhibits an exponential and random distribution for the laser beam and ambient light, respectively. The average interval τ_{Laser} between two adjacent laser photons is expected to the reciprocal of the photon arrival rate, i.e., $\tau_{Laser} = 1/R_{Laser}$. Similarly, the average interval τ_{Amb} equals to $1/R_{Amb}$ for ambient photons. In terms of the photon arrival rates given in Equations (7) and (9), the arrival time of the individual photon can be modeled.

TABLE 1
System and Simulation Parameters Used in the Behavioral Model

Parameter	Description	Value
P_{Source}	Laser source power	400 W
E_{Amb}	Power density of ambient sunlight	10 Klux
D	Aperture diameter	1.5625 mm
f	Focal length	12.5 mm
α_x	Laser divergence angle (H)	5 ^{o}
α_y	Laser divergence angle (V)	0.1 ^{o}
Γ_T	Target reflectance	50 %
T_o	Optics efficiency	50 %
A_{Pix}	Pixel area	0.01 mm^2
λ	Laser wavelength	905 nm
t_{jitter}	Laser jitter time	80 ps
FF	Fill factor	10 %
PDE	Photon detection efficiency	8 %

3. Verilog-A Model Implementation

The derived theory model of the photon arrival rates was implemented in Verilog-A HDL. Above all, the arrival time of the first laser photon reflected by the target is calculated according to the target distance and light speed. However, the first photon arrival time exhibits little uncertainty due to the laser timing jitter. To illustrate the impact of this effect, a Gauss distribution function is applied to obtain the statistical arrival time. We take the laser jitter time as a mean value of Gauss distribution function $rdist_normal (seed, 0, mean) to return a random number, marking the arriving time of the first received laser photon. Then, taking this arrival time of the first photon as a starting point and using the expected average interval τ_{Laser} as a mean value, an exponential distribution function $rdist_exponential (seed, mean) is adapted to record the arrival time of a series of laser photons within a specified laser pulse duration. Meanwhile, we make use of a random distribution time function $random (seed) with the expected average interval τ_{Amb} as a mean value to randomly generate ambient photons in the whole TOF measurement window. Finally, the laser photon signals are merged with the ambient photon signals. One example of the Verilog-A HDL codes for modeling photon arrival events is illustrated in Fig. 2.

4. Verilog-A Model Simulation and Validation

The Verilog-A model was operated on Cadence Spectre simulator to validate the feasibility of model simulation. The used key model parameters are listed in Table 1. The emission power and wavelength of laser source are assumed to 400 W and 905 nm. The divergence angles of the laser beam along horizontal and vertical directions are set to 5° and 0.1°, respectively. A standard optical lens with 12.5 mm focal length and 1.5625 mm aperture diameter is used. The pixel of the SPAD detector occupies an area of 0.01 mm^2 with a fill factor of 10% and a PDE of 8%. A Lambertian reflection coefficient of 50% is assumed for a target.

Fig. 3 illustrates the photon arrival time distribution in a 100 ns measurement window by model simulation. Here, the distance of the target is assumed to 7.5 m. The duration and time jitter of laser pulses is assumed to 15 ns and 80 ps, respectively. Fig. 3(a) shows the arrival time of the first laser photon reflected by the target is around 50 ns corresponding to the target distance of 7.5 m, which exhibits a Gauss statistical distribution due to the time jitter of laser emission. Once the first laser photon arrives, taking this arrival time as a start point, a series of laser photons with 200 MHz arrival rate appear continuously, showing an exponential distribution in the duration of the laser pulse, as shown in Fig. 3(b). Additionally, Fig. 3(c) displays the arrival time of ambient photons

```
module photon_arrival_time (photon_out);
/********************** define parameter**********************/
parameter real Psource = 400;                    //Laser power
parameter real FT = 0.5;                         //Target reflectance
parameter real TO = 0.5;                         //Optics efficiency
parameter real Apix = 0.01e-6;                   //Pixel area
parameter real Lamdar = 905e-9;                  //Laser wavelength
parameter real FF = 0.1;                         //Fill Factor
parameter real PDE = 0.08;                       //Photon detect efficiency
parameter real f = 12.5;                         //Focal length
parameter real D = 1.5625;                       // Aperture diameter
parameter real f1 = 12.5/1.5625;                 // f/D
parameter real d = 7.5;                          //d is the target distance
parameter real ax = 5;                           //Laser source opening angle(H)
parameter real ay = 0.1;                         //Laser source opening angle(V)
parameter real EAmb = 10000;                     //Ambient light density
parameter real tjitter=80                        //Laser jitter time
parameter real thresh = 0.9;                     //Define trigger threshold voltage
/**********************define function**************************/
`define Esource Psource/(4*d*d*asin(sin(ax)*sin(ay)))
`define Rlaser (`Esource*FT*TO*Apix*Lamdar*FF*PDE)/(8*f1*f1*h*c)
`define RAmb (FT*TO*Apixel*FF* EAmb *Lamdar)/(8*(f1*f1)*h*c*683);
`define seed random_value
/**********************photon arrival**************************/
//Generate the first arriving laser photon with gauss distribution
@(timer(random_time))
begin
gauss_reg = $rdist_normal(gauss_seed,0, `Tjitter);
end
@(timer(photon_gauss_time + gauss_reg))
begin
gauss_out = 1;
end
V(out)<+transition(gauss_out*1.8,td,tt);          // Generate the first laser photon
.......
//Generate laser photons with exponential distribution
exp_out = 0;
exp_reg = $rdist_exponential(`seed,`Rlaser); //Return exponential distribution value
random_time_n = $random(seed);
@(cross(V(gauss_out)-thresh,1))                   //Judge the first laser photon coming
begin
photon_arrival_time = $abstime;
end
@(timer(random_time_n))
begin
exp_reg_m = exp_reg;                              // Mark the exponential distribution time
end
@(timer(photon_arrival_time + exp_reg_m))
begin
exp_out = 1;
end
V(out)<+transition(exp_out*1.8,td,tt);            // Generate exponentially distributed photons
.......
//Generate ambient photons with random distribution
Amb_out = 0;
Amb_random = ($random%)`RAmb                      //Return random distribution value
@(timer(Amb_random))
begin
Amb_out = 1;
end
V(out)<+transition(Amb_out*1.8,td,tt);            // Generate randomly distributed photons
.......
photon_reg = Amb_out || exp_out;                  // Merge laser and ambient photons
assign photon_out = photon_reg
endmodule
```

Fig. 2. Verilog-A HDL codes for modeling photon arrival events.

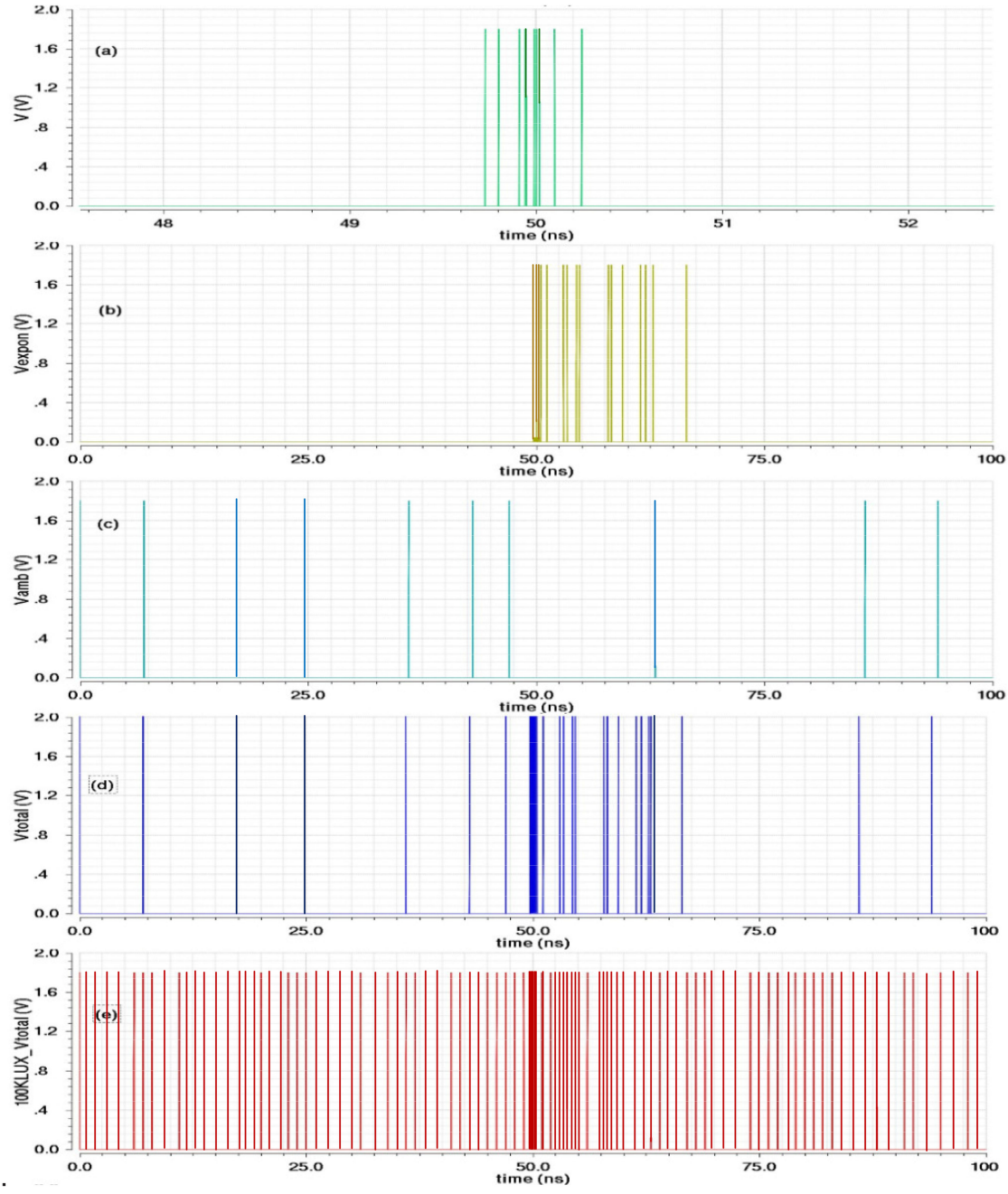

Fig. 3. Photon arrival time distribution in a 100 ns detectable window by model simulation. (a) First arriving laser photon with Gauss distribution. (b) Laser photons with an exponential distribution. (c) Random ambient photons at 10 klux. (d) The merged laser and ambient photons at the ambient light of 10 klux. (e) The merged laser and ambient photons at the ambient light of 100 klux.

in a 100 ns detectable window under the ambient light density of 10 klux. It is observed that the ambient photons occur randomly across the whole detectable window with the arrival rate of about 70 MHz. Finally, the laser and ambient photons are merged, as shown in Fig. 3(d). It is noticed that if the ambient light density is further enhanced to 100 klux, the arrival rate of ambient photons will increase significantly, as depicted in Fig. 3(e). Hence, it will become more difficult to detect the first arrival laser photon from a plurality of ambient photons.

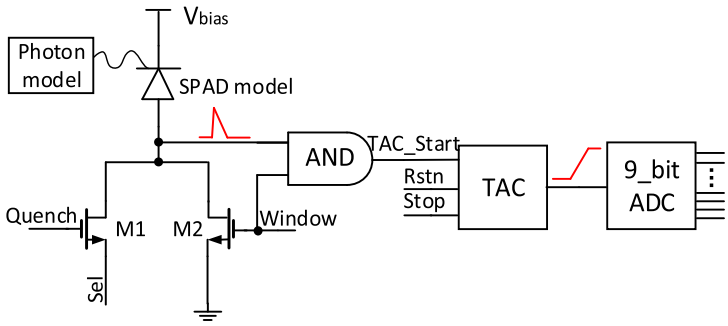

Fig. 4. Diagram of a direct TOF measurement system for model circuit simulation.

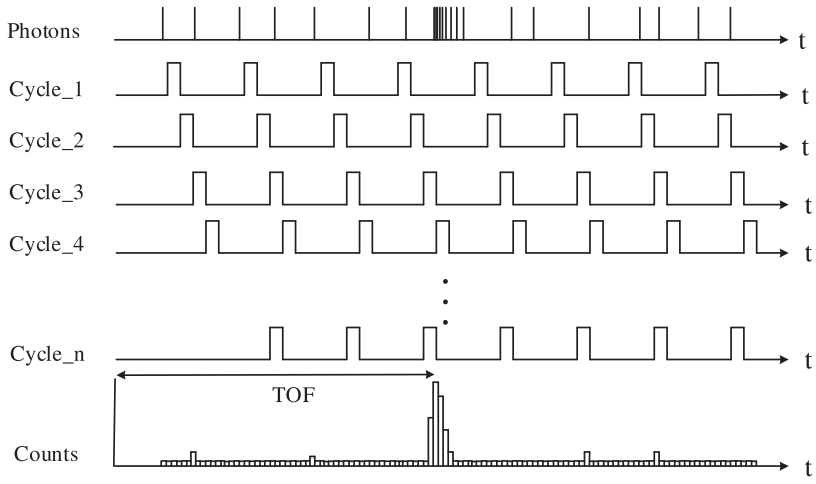

Fig. 5. Operating principle of the dTOF measurement. The arriving photons are detected over many cycles. In every cycle, the SPAD is ready to detect a photon in a shifting timing window.

The TOF circuit simulation is further carried out to verify the accuracy of the behavioral model. Fig. 4 shows a direct TOF measurement system, including a SPAD detector, a gated quench circuit, and a TAC circuit. Here, an accurate behavioral SPAD model is used to emulate the statistical performance of the SPAD device, including avalanche triggering, dark counts and after-pulsing phenomenon [15], [16]. In our work, the dark count rate and the after-pulsing rate of the SPAD device model are lower than the photon arrival rates, so they pose little influence on the TOF measurement. The input photon signals of the SPAD device model are provided by the proposed photon model. The gated quenching circuit consists of two transistors of M1 and M2 and one AND gate. The quenching and recharging operations are controlled by 'Quench' and 'Window' signals [3], [17]. The TAC circuit features a 200 ps timing resolution in a full-scale range of 100 ns. The time-to-amplitude conversion is started by photon avalanche signal 'TAC_Start' and stopped by global 'Stop' signal. Ultimately, the output result of the TAC is converted into 9-bit digital signals.

To suppress the influences of ambient illumination, the dead time of SPAD device and other statistical variations in the LIDAR system, the TOF measurements should be operated repeatedly over hundreds or even thousands of cycles. Fig. 5 presents the operating principle of the TOF measurement with multiple cycles in this work. To cover the whole time span, in every cycle, the SPAD is ready to detect a photon in a shifting timing window. The obtained photon arrival time values are collected in a histogram over many cycles. In terms of the histogram peak, the photon flight time can be calculated by using a software algorithm.

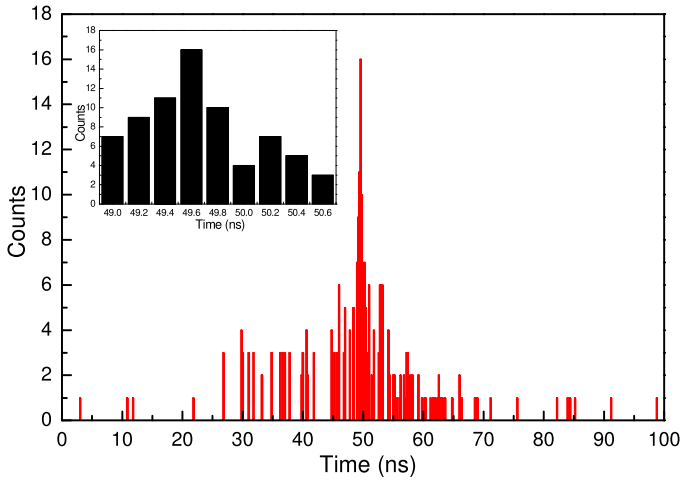

Fig. 6. Accumulated counts of different photon arrival time by model simulation. Simulated data with 300 cycles is collected in the histogram.

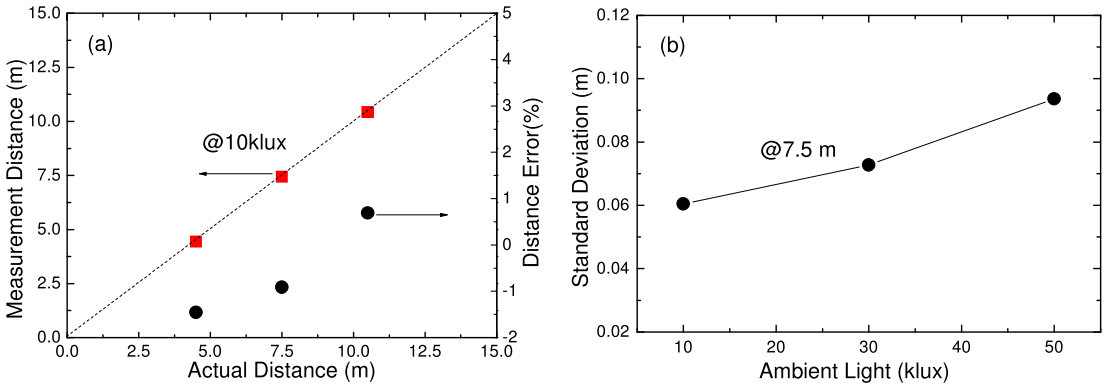

Fig. 7. (a) Distance error for three target distances at the ambient light density of 10 klux. (b) Standard deviation of measurement distance as a function of ambient light density by model simulation.

Fig. 6 intuitively depict a simulation example of the accumulated photon arrival time at the ambient illumination density of 10 Klux. Here, the photon arrival time over 300 cycles is collected in a histogram with a 200 ps bin width. In this histogram, the arrival time of the detected photons is mainly concentrated around 50 ns. Furthermore, a small number of ambient photons are accumulated as well across the whole 100 ns time span. More clearly, a histogram peak is found at 49.6 ns, as displayed in the inset picture of Fig. 6, indicating the arriving time of the first laser photon reflected by the target. It means the target distance is about 7.44 m, which is very close to the actual distance of 7.5 m.

Fig. 7(a) shows the TOF measurement precision by model simulation for three target distances at the ambient light density of 10 Klux. The measurement distances are very proximate to the actual values and the measurement error is less than 1.46% within 10.5 m distance. Fig. 7(b) illustrates the standard deviation of measurement distance versus ambient light density. It is obviously found that the stronger the ambient illumination, the larger the measurement standard deviation. As the ambient light density is enhanced from 10 to 50 klux, the standard deviation of the measurement distance is increased from 6 cm to 9 cm for 7.5 m target distance. This is due to the fact that the increased photon arrival rate of the ambient light seriously affects the TOF measurement of the first arriving laser photon. The obtained simulation results show good accordance with the

actual situation [18], which validates the high accuracy of the proposed model. It suggests that this behavioral model is very suitable for the TOF-related circuit simulation and can be used to accurately predict the performance of a LIDAR system.

5. Conclusions

In this paper, a novel behavioral model is proposed to estimate the statistical photon arrival time for SPAD-based TOF measurement system simulation. A theoretical calculation model is firstly derived and illustrated with the full consideration of the performance parameters of LIDAR system, such as laser source, ambient illumination, optics, SPAD device for the accurate prediction of photon arrival rate. The proposed theoretical photon arrival rate model was then realized with Verilog-A HDL. For the first time, the LIDAR system level circuit simulation is carried out on the commercial simulator by means of the presented Verilog-A model. The circuit simulation indicates that the photon flight time corresponding to the measurement distance can be accurately assessed, proving the feasibility and accuracy of the model. The proposed behavioral model enables LIDAR system level circuit simulation and provides a useful candidate tool for the design and optimization of the SPAD-based TOF measurement circuits.

References

[1] I. Takai, H. Matsubara, M. Soga, M. Ohta, M. Ogawa and T. Yamashita, "Single-photon avalanche diode with enhanced NIR-sensitivity for automotive LIDAR systems," *Sensors*, vol. 16, 2016, Art. no. 459.

[2] M. Beer *et al.*, "SPAD-based flash LiDAR sensor with high ambient light rejection for automotive applications," *Proc. SPIE*, vol. 10540, 2018, Art. no. 105402G.

[3] F. Villa *et al.*, "SPAD smart pixel for time-of-flight and time-correlated single-photon counting measurements," *IEEE Photon. J.*, vol. 4, no. 3, pp. 795–804, Jun. 2012.

[4] C. Niclass, M. Soga, H. Matsubara, S. Kato, and M. Kagami, "A 100-m-range 10-frame/s 340 $\times$ 96-pixel time-of-flight depth sensor in 0.18-μm CMOS," *IEEE J. Solid-State Circuits*, vol. 48, no. 2, pp. 559–572, Feb. 2013.

[5] D. Bronzi, Y. Zou, F. Villa, S. Tisa, A. Tosi, and F. Zappa, "Automotive three-dimensional vision, a single-photon counting SPAD camera," *IEEE Trans. Intell. Transp. Syst.*, vol. 17, no. 3, pp. 782–795, Mar. 2016.

[6] R. Lussana, F. Villa, A. D. Mora, D. Contini, A. Tosi, and F. Zapp, "Enhanced single-photon time-of-flight 3D ranging," *Opt. Exp.*, vol. 23, no. 19, pp. 24962–24973, 2015.

[7] D. Bronzi, F. Villa, and S. Tisa, "100 000 Frames/s 64 $\times$ 32 single-photon detector array for 2-D imaging and 3-D ranging," *IEEE J. Sel. Topics Quantum Electron.*, vol. 20, no. 6, pp. 354–363, Nov./Dec. 2014.

[8] C. Niclass, C. Favi, T. Kluter, M. Gersbach, and E. Charbon, "A 128 $\times$ 128 single-photon image sensor with column-level 10-bit time-to digital converter array," *IEEE J. Solid-State Circuits*, vol. 43, no. 12, pp. 2977–2989, Dec. 2008.

[9] F. Villa *et al.*, "CMOS imager with 1024 SPADs and TDCs for single photon timing and 3-D time-of-flight," *IEEE J. Sel. Topics Quantum Electron.*, vol. 20, no. 6, pp. 364–373, Nov./Dec. 2014.

[10] M. Crotti, I. Rech, and M. Ghioni, "Four channel, 40 ps resolution, fully integrated time-to-amplitude converter for time-resolved photon counting," *IEEE J. Solid-State Circuits*, vol. 47, no. 3, pp. 699–708, Mar. 2012.

[11] M. Beer, O. M. Schrey, B. J. Hosticka, and R. Kokozinski, "Modelling of SPAD-based time-of-flight measurement techniques," in *Proc.Eur. Con. Circuit Theory Des.*, 2017, pp. 1–4.

[12] M. Beer, B. J. Hosticka, and R. Kokozinski, "SPAD-Based 3D Sensors for high ambient illumination," in *Proc. 12th Conf. Ph.D. Res.Microelectron. Electron.*, 2016, pp. 1–4.

[13] S. Gnecchi and C. Jackson, "A 1 $\times$ 16 SiPM array for automotive 3D Imaging LiDAR Systems," in *Proc. Int. Image Sensor Workshop*, 2017, pp. 133–136.

[14] F. Arvani and T. C. Carusone, "Direct time-of-flight TCSPC analytical modeling including dead-time effects," in *Proc. IEEE Int. Symp. Circuits Syst.*, 2018, pp. 1–4.

[15] Y. Xu, T. Zhao, and D. Li, "An accurate behavioral model for single-photon avalanche diode statistical performance simulation," *Superlattices Microstruct.*, vol. 113, no. 1, pp. 635–643, 2018.

[16] Y. Xu, P. Xiang, and X. Xie, "Comprehensive understanding of dark count mechanisms of single-photon avalanche diodes fabricated in deep sub-micron CMOS technologies," *Solid-State Electron.*, vol. 129, pp. 168–174, 2017.

[17] D. Portaluppi, E. Conca, and F. Villa, "32 $\times$ 32 CMOS SPAD imager for gated imaging, photon timing, and photon coincidence," *IEEE J. Sel. Topics Quantum Electron.*, vol. 24, no. 2, Mar./Apr. 2018, Art. no. 3800706.

[18] H. Akita, I. Takai, K. Azuma, T. Hata, and N. Ozaki, "An Imager using 2-D single-photon avalanche diode array in 0.18-μm CMOS for Automotive LIDAR application," in *Proc. Symp. VLSI Circuits*, 2017, pp. C290–C291.